RESEARCH PAPER

Mechanism governing separation in microfluidic pinched flow fractionation devices

Sumedh R. Risbud · German Drazer

Abstract We present a computational investigation of the mechanism governing *size-based* particle separation in microfluidic pinched flow fractionation. We study the behavior of particles moving through a pinching gap (i.e., a constriction in the aperture of a channel) in the Stokes regime (negligible fluid and particle inertia) as a function of particle size. The constriction aperture is created by a plane wall and spherical obstacle, and emulates the pinching segment in pinched flow fractionation devices. The simulation results show that the distance of closest approach between the particle and obstacle surfaces (along a trajectory) decreases with increasing particle size. We then use the distance of closest approach to investigate the effect of short-range repulsive non-hydrodynamic interactions (e.g., solid-solid contact due to surface roughness, electrostatic, or steric repulsion, etc.). We define a *critical trajectory* as the one in which the minimum particle–obstacle separation is equal to the range of the non-hydrodynamic interactions. The results further show that the initial offset of the critical trajectory (defined as the critical offset) increases with particle size. We interpret the variation of the critical offset with particle size as the basis for size-based microfluidic separation in pinched flow fractionation. We also compare the effect of different driving fields on the particle trajectories; we simulate a constant force driving the particles in a quiescent fluid as well as a freely suspended particles in a pressure-driven flow. We observe that the particles approach closer to the obstacle when driven by a constant force, than those freely suspended in a pressure driven flow (for the same initial offset). On the other hand, the increment in the critical offset (as a function of particle size) is larger in the pressure-driven case than in the force-driven case. Thus, pressure-driven particle separation using pinched flow fractionation would prove more effective than its force-driven counterpart (e.g., particles settling under gravity through a pinching gap).

Keywords Microfluidic separations · Pinched flow fractionation · Trajectory analysis

S. R. Risbud
Department of Chemical and Biomolecular Engineering, Johns Hopkins University, Baltimore 21218, MD, USA

Present Address:
S. R. Risbud
Department of Chemical Engineering, Massachusetts Institute of Technology, Cambridge 02139, MA, USA

G. Drazer (✉)
Department of Mechanical and Aerospace Engineering, Rutgers, The State University of New Jersey, Piscataway 08854, NJ, USA
e-mail: german.drazer@rutgers.edu

1 Introduction

A particularly attractive microfluidic separation technique would be able to exploit the differences in the interactions of the particles with the geometric features embedded within the channels of a micro-device, without the need of an external field. A few examples of such fluidic-only separation methods include the following: size-exclusion, entropic trapping (Han and Craighead 2000), deterministic lateral displacement (Huang et al. 2004), and pinched flow fractionation [PFF, Yamada et al. (2004)]. PFF is a relatively simple method, in which species entering a channel constriction exit into a sudden expansion at different positions across the channel. As a result of its simplicity and promise, numerous variants of PFF have emerged within the last decade (Lee et al. 2011; Larsen et al. 2008; Maenaka et al. 2008; Morijiri et al. 2011; Vig and Kristensen 2008).

The separation of flow streamlines coming out of the constriction was originally suggested as the basis of PFF (Yamada et al. 2004). This explanation, however, does not take into account particle-wall hydrodynamic interactions. Two factors indicate the need to consider hydrodynamic interactions to determine the particle motion through a constriction. First, the particles are similar in size to the width of the constriction and, therefore, cannot be considered as tracer particles advected by the flow (Mortensen 2007; Shardt et al. 2012; Ashley et al. 2013). Second, as the particles move through the constriction, the surface-to-surface separation between the particles and the channel wall tends to become much smaller than the size of the particles, and lubrication forces can play a significant role. Studying the motion of a particle through a constriction is also relevant in the context of certain particle focusing methods (Faivre et al. 2006; Xuan et al. 2010) and micro-models of porous media employed in particle deposition studies (Wyss et al. 2006; Mustin and Stoeber 2010).

We have recently studied the relationship between the initial offset in a particle trajectory (b_{in} in Fig. 1b) and the minimum surface-to-surface separation between the particle and the obstacle along the trajectory. We have shown that even a moderate initial offset in a particle trajectory (say, comparable to the particle radius) leads to surface-to-surface separations that are significantly smaller, e.g., $O(100 \text{ nm})$ between a particle and an obstacle of micrometer size (Risbud and Drazer 2013). The occurrence of such small surface-to-surface separations highlights the importance of short-range non-hydrodynamic interactions and suggests the minimum separation as the relevant length scale to compare with the range of these forces. Such interactions can be modeled using a hard-wall repulsion, which leads to the definition of a *critical offset*, i.e., the smallest initial offset that results in a fore-aft symmetric trajectory (Balvin et al. 2009; Frechette and Drazer 2009; Risbud and Drazer 2013). We have also shown that the relationship between the critical offset and the range of repulsive interactions is the same as that between the initial offset and the minimum surface-to-surface separation (Frechette and Drazer 2009; Risbud and Drazer 2013). In previous lattice Boltzmann simulations (Risbud et al. (2013), henceforth *paper I*), we studied the trajectory followed by a spherical particle as it passes through a constriction created by a spherical obstacle of *the same size* and a plane wall. We showed that, for the same initial offset, a particle reaches closer to the obstacle as the constriction aperture decreases. Therefore, the critical offset increases with decreasing constriction aperture.

In this article, we investigate the motion of particles of *various sizes* as they move through a constriction. We show
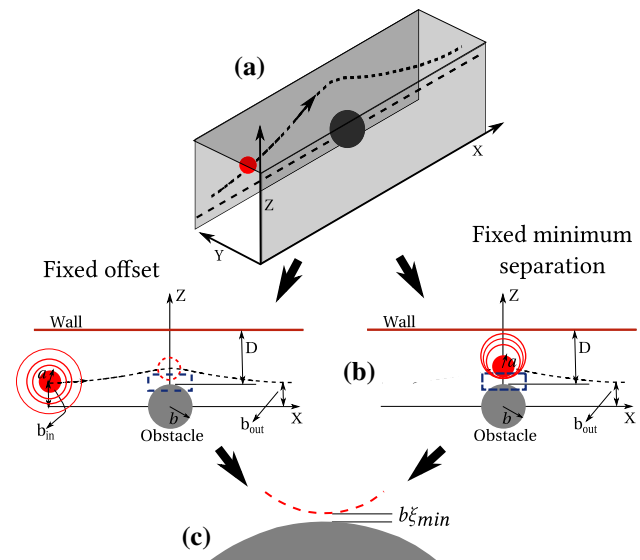

Fig. 1 Simulation box and relevant length scales. **a** The simulation box with the coordinate system. Two parallel walls perpendicular to the *Y*-axis form a channel in all simulations. **b** This is an enlarged view of the relevant part of the simulation box. (*left*) In *fixed offset* simulations, the initial position of all particle centers is the same (as depicted by the *concentric circles*). The initial and the final offsets (b_{in}, b_{out}) are indicated, along with the particle and obstacle radii, and the size of the constriction aperture *D*. The *dashed circle* shows the position of the closest approach along the particle trajectory. (*right*) In *fixed-ξ_{min}* simulations, the particles begin their motion just before the apex of their trajectories and attain the same minimum surface-to-surface separation (as depicted by the *internally tangential circles*). The radii of the particle and the obstacle are *a* and *b*, respectively. **c** Close-up of the region enclosed by a *dashed box* in (**b**) highlighting the minimum separation between particle and obstacle surfaces

that irreversible particle-wall interactions could lead to *size-based separation* at low Reynolds number. Particularly, we show that particles of different sizes exhibit different extents of lateral displacement as they move through a constriction. We present the results of lattice Boltzmann simulations for various particle-obstacle aspect ratios and sizes of the constriction aperture in the Stokes regime (negligible particle and fluid inertia). We also investigate the dependence of the critical offset on the driving field; we simulate the trajectories resulting from a constant force driving the particles in a quiescent fluid as well as those corresponding to freely suspended particles driven by a pressure-driven flow. Based on the hard-wall model, we show that larger particles exhibit a larger critical offset in the presence of a non-hydrodynamic repulsion of fixed range. Therefore, size-based separation as a result of particles moving through a constriction can be qualitatively explained through this study. Further, we show that decreasing the constriction aperture also increases the critical offset, with the increment being larger for the case of a pressure-driven flow carrying the particles.

The article is organized as follows: In Sect. 2, we introduce the system under investigation, as well as the nature of the simulations carried out in this study. In Sect. 3, we discuss the hard-core model for short-range repulsive non-hydrodynamic interactions. In Sects. 4.1 and 4.2, we present the results of the simulations, and in Sect. 4.3, we discuss size-based separation using the results.

2 The system

Figure 1 depicts the system studied in this work. We consider a suspended spherical particle of radius a (diameter d) negotiating a fixed spherical obstacle of radius b along the positive x-axis. We use the lattice Boltzmann method (*susp3d*) (Ladd 1994a, b; Nguyen and Ladd 2002). The simulation box is outlined in Fig. 1a and has dimensions $x \times y \times z \equiv 240 \times 60 \times 140$ lattice units. The two walls perpendicular to the y-axis form a channel (henceforth, 'side walls' or channel walls). The plane of motion is the midplane of the channel, parallel to the xz-plane. The particle motion is planar, confined to the midplane due to the symmetry of the problem. The particle trajectory passes through a constriction of minimum aperture D, created by the plane wall perpendicular to the positive z-axis (henceforth, the 'top' wall) between itself and the obstacle surface (Fig. 1b). The initial (upstream) and final (downstream) offsets in the particle trajectory are denoted by b_{in} and b_{out}, respectively. Since we are investigating particle trajectories in the Stokes regime (i.e., negligible fluid as well as particle inertia), the trajectories are fore-aft symmetric and the two offsets are equal ($b_{in} = b_{out}$). The minimum surface-to-surface separation between a particle and the obstacle is $b\xi_{min}$ as shown in Fig. 1c. The no-slip boundary condition is imposed on all solid boundaries, while a periodic boundary condition is imposed on the faces of the simulation box perpendicular to the x-axis. In the absence of the top wall, periodic boundary condition is also imposed on the faces perpendicular to the z-axis. We vary (reduce) the constriction aperture by translating the obstacle center along z-axis toward the top wall.

We have performed two sets of simulations (Fig. 1b): First, we investigate trajectories that have the same initial offset $b_{in} = 30$ lattice units, with an obstacle of radius $b = 10$ lattice units (henceforth, *fixed offset* simulations). Second, we study trajectories that attain the same minimum separation between particle and obstacle surfaces (1 lattice unit), with an obstacle of radius $b = 20$ lattice units (henceforth, *fixed-ξ_{min}* simulations). We use a larger obstacle in the fixed-ξ_{min} simulations to achieve a smaller dimensionless minimum separation (1 lattice unit $\equiv \xi_{min} = 5 \times 10^{-2}$). The fixed offset simulations exhibit different minimum separations, whereas the fixed-ξ_{min}

simulations exhibit different final offsets. Both cases probe the dependence of the respective variables on the constriction aperture and particle size. We investigate the effect of two driving fields: a constant force driving the particles in a quiescent fluid, and freely suspended particles driven by a pressure-driven flow. In both sets of simulations, the obstacle radius serves as the characteristic length scale of the problem. As mentioned earlier, the magnitudes of particle as well as fluid inertia are negligible in all simulations (Re $\sim O(10^{-2}) - O(10^{-3})$ and St $\sim O(10^{-3}) - O(10^{-4})$).

The particle-to-obstacle aspect ratio $\alpha = a/b$ and the dimensionless constriction aperture $\Delta = D/b$ form the parameter space relevant to this study. We use four different particle sizes, $a = 5, 10, 15, 20$ lattice units, yielding the particle-to-obstacle aspect ratios $\alpha = \frac{1}{2}, 1, \frac{3}{2}, 2$ for fixed offset simulations, and $\alpha = \frac{1}{4}, \frac{1}{2}, \frac{3}{4}, 1$ for fixed-ξ_{min} simulations. Note that the values of α are different for the two sets of simulations due to different obstacle radii.

In the fixed offset simulations, we investigate the constriction apertures $D = 60$ and $D = 50$ lattice units ($\Delta = 6$ decreasing to $\Delta = 5$) and also investigate the trajectories in the absence of the top wall (the latter corresponding to the absence of a constriction). For the fixed-ξ_{min} simulations, the sizes of the constriction apertures are $D = 98, 78, 58,$ and 45 lattice units ($\Delta = 4.9, 3.9, 2.9, 2.25$). The initial and final offsets are noted at $x = -100$ and $x = 100$ lattice units, respectively. For each fixed-ξ_{min} simulation, the initial z-coordinate of the particle center is calculated such that approximately the same minimum surface-to-surface separation is attained by particles of all sizes.

As discussed in Sect. 1, the minimum separation attained along a particle trajectory (ξ_{min} in Fig. 1c) serves as the length scale to be compared with the range of short-range non-hydrodynamic interactions to estimate their effect on the trajectory. Thus, in what follows, we present the results obtained for the minimum separation ξ_{min} as a function of the particle-obstacle aspect ratio and constriction aperture.

3 The minimum separation and the model for non-hydrodynamic interactions

Following paper I, we model the short-range repulsive (irreversible) interactions between a particle–obstacle pair (such as solid–solid contact due to surface roughness), as a hard-wall potential creating a hard-core shell of effective range ε, such that, any surface-to-surface separation between the particle and the obstacle less than ε (i.e., $\xi_{min} < \varepsilon$) is not attainable. We have established that this model leads to the definition of a critical offset b_c that depends on the range of the non-hydrodynamic interactions
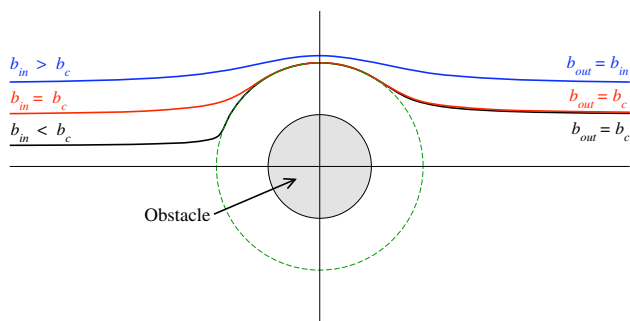
Fig. 2 Three types of particle trajectories in the presence of non-hydrodynamic interactions in the Stokes regime. Reproduced from Balvin et al. (2009)

(Frechette and Drazer 2009; Risbud and Drazer 2013). The existence of the critical offset can be explained as follows: The presence of non-hydrodynamic interactions with a dimensionless range ε around the obstacle prevents the particle surface to approach the obstacle surface closer than ε. Then, the particle trajectories corresponding to $\xi_{\min} > \varepsilon$ are unaffected by the presence of the non-hydrodynamic interactions (see the top-most trajectory in Fig. 2). The trajectory that corresponds to a minimum surface-to-surface separation $\xi_{\min} = \varepsilon$ serves as the *critical trajectory* (see the middle trajectory in Fig. 2). Finally, the trajectories that would have approached a minimum surface-to-surface separation $\xi_{\min} < \varepsilon$ in the absence of the non-hydrodynamic interactions are forced to circumnavigate the obstacle while maintaining a constant separation equal to ε due to the hard-wall repulsion. These trajectories collapse onto the critical trajectory downstream of the obstacle (see the bottom-most trajectory in Fig. 2). Alternatively, the critical offset b_c can be defined as the *smallest initial offset that results in a symmetric particle trajectory around the obstacle*. Further, since the minimum separation attained by a particle moving along the critical trajectory is exactly $\xi_{\min} = \varepsilon$, from the above definition, the relationship between b_c and ε is the same as that between $b_{\rm in}$ and $\xi_{\min}$ (Frechette and Drazer 2009; Bowman et al. 2012; Devendra and Drazer 2012).

4 Results and discussion

4.1 Fixed offset simulations

Figure 3 shows $\xi_{\min}$ as a function of the particle size, for the two different driving fields. In Fig. 3a, we plot the case when the particle is driven by a constant force in a quiescent fluid. Figure 3b, on the other hand, represents the pressure-driven case. In both cases, we observe that $\xi_{\min}$ decreases with increasing particle size for a constant constriction aperture and also with decreasing constriction

aperture for a fixed particle size. The latter observation extends the results presented in paper I (i.e., results obtained for a particle of the same size as the obstacle). Note that, we have shown via theoretical calculations that the minimum separation as a function of the particle size reverses its trend for asymptotically small separations in the absence of a constriction ($\xi_{\min} \ll O(10^{-7})$), so that smaller particles reach closer to the obstacle (Risbud and Drazer 2013). However, these separations are not relevant in practice, since they are much smaller than the range of typical irreversible forces for micrometer size particles. Comparing Fig. 3a, b, we note that a given particle reaches closer to the obstacle when moving due to a constant force in a quiescent fluid, than in a pressure-driven flow. This is consistent with our analysis based on the hydrodynamic mobility of a sphere moving around an obstacle, in the absence of the wall creating the constriction (Risbud and Drazer 2013). In summary, we conclude that *the particles reach closer to the obstacle upon decreasing the constriction aperture or increasing the particle size*.

Let us now discuss the implications of the hard-wall potential model. As mentioned earlier in Sect. 2, all trajectories in this set have the same initial offset $b_{\rm in}$, and the obstacle radius b is constant ($b = 10$ lattice units). Let the corresponding critical offset be $b_{c0} < b_{\rm in}$ for a given particle radius and constriction aperture $D = D_0$. We first discuss the effect of decreasing the constriction aperture keeping the particle radius constant (i.e., following the direction of the downward arrow in Fig. 3). Since we have observed that $\xi_{\min}$ decreases with the constriction aperture, for a sufficiently small aperture $D' < D_0$, the minimum separation would, in principle, reach the range of the non-hydrodynamic interactions ($\xi_{\min} = \varepsilon_0$). Correspondingly,
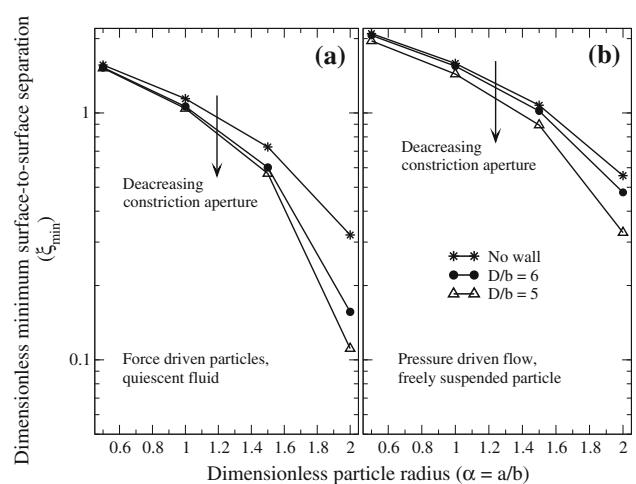

Fig. 3 The dimensionless minimum separation $\xi_{\min}$ versus the dimensionless particle radius α for different driving fields: **a** A constant force acting on the particle in a quiescent fluid, **b** a constant pressure drop acting on the fluid with a freely suspended particle

the critical offset would increase from $b_{c0} < b_{in}$ to $b'_c = b_{in}$. In other words, *for a given particle radius, the corresponding critical offset increases with decreasing constriction aperture*. We note that this result is in qualitative agreement with previous experiments (Luo et al. 2011) and extends the results obtained for $\alpha = 1$ (paper I) to $\alpha \neq 1$.

The above inference was drawn using a fixed α and varying the constriction aperture Δ. An analogous argument can be made using the particle radius a as a variable, wherein the minimum separation is observed to decrease with increasing particle radius. Therefore, *a decrease in ξ_{min} due to increasing the particle radius for a given constriction aperture, results in an increase in the critical offset b_c in the presence of non-hydrodynamic interactions*. However, in this case, we need to assume that the non-hydrodynamic interactions have a fixed dimensionless range $\varepsilon = \varepsilon_0$, set by the obstacle and independent of particle size.

Therefore, in general, a decrease in the minimum separation ($\xi_{min} \downarrow$) in the absence of non-hydrodynamic interactions corresponds to an increase in the critical offset ($b_c \uparrow$) in their presence. In the following section, we indeed show this to be the case by direct verification using the fixed-ξ_{min} simulations.

4.2 Fixed-ξ_{min} simulations

The objective of this set of simulations is to investigate the dependence of b_{out} on the parameters of the problem when the minimum separation is kept constant. Specifically, we perform simulations that correspond to a minimum separation of 1 lattice unit, i.e., $\varepsilon = 1/20 = 0.05$ (for $b = 20$ lattice units). We know that the functional relationship between b_{out} (same as b_{in} in Stokes regime) and ξ_{min} is the same as that between b_c and ε (Risbud and Drazer 2013). Therefore, the final offsets b_{out} corresponding to the various trajectories obtained in these simulations are the values of the critical offset b_c corresponding to $\varepsilon = 0.05$.

However, as shown in Fig. 4, our simulated trajectories attain the minimum separation of 0.05 only approximately. Therefore, for each particle size, we compute the final offset corresponding to $\xi_{min} = 0.05$ by linear interpolation between two independent simulations for which ξ_{min} is greater/smaller than 0.05, leading to the error bars shown in Fig. 5. It is evident from Fig. 5 that the critical offset increases with the size of the particle (an inference already stated in Sect. 4.1), qualitatively corroborating earlier experimental observations (Luo et al. 2011).

We again compare the effect of the field driving the particle past the obstacle. Figure 5a corresponds to a particle driven by a constant force, whereas Fig. 5b shows the results for pressure-driven flow. We observe that the driving field significantly affects the critical offset: In general, higher critical offsets are observed for the case of a constant force driving the particle in a quiescent fluid. This
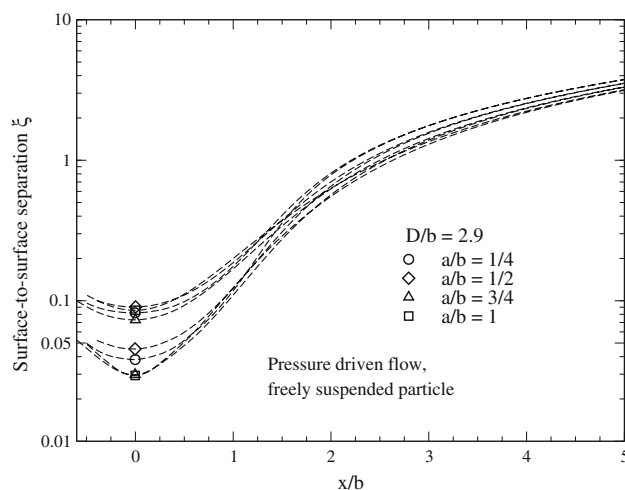

Fig. 4 The dimensionless surface-to-surface separation ξ between the particle and the obstacle as a function of the dimensionless x-coordinate. As mentioned in the text, two simulations are carried out for each particle size for the purposes of linear interpolation, such that both attain minimum separation close to $\xi_{min} = 0.05$ (one less than 0.05, and the other greater than 0.05). Four *different line-styles* correspond to the four particle sizes used in the simulations. The two groups of trajectories (one corresponding to $\xi_{min} > 0.05$ and the other corresponding to $\xi_{min} < 0.05$) can be clearly seen in the figure. This particular plot depicts the case when $\Delta = 2.9$ and the particles are carried around the obstacle by a pressure-driven flow

is consistent with the argument presented in Sect. 4.1 that a given particle reaches closer to the obstacle when driven by a constant force compared to a pressure-driven flow.

Figure 5 also shows that decreasing the constriction aperture affects the case of fluid flow more than the case of a constant force driving the particles. Further, in previous experimental findings, we have observed that the increment in the critical offset itself increases with particle size (Luo et al. 2011). However, the increment observed in the experiments is smaller than the resolution of the current data (i.e., the error bars depicted in the figure). Therefore, we cannot conclusively compare the experimental findings with the available simulation data.

4.3 Size-based separation

We have established that the critical offset b_c increases with increasing particle size, and/or decreasing the constriction aperture. Particularly, we have concluded that for the same constriction aperture, two particles of different sizes would exhibit different critical offsets. From the perspective of size-based separations, and for the sake of specificity, let b_{c1} and b_{c2} be the values of these critical offsets for particles of radii a_1 and a_2, respectively. If $a_1 < a_2$, then from the previous discussion, it follows that $b_{c1} < b_{c2}$, assuming the same range of non-hydrodynamic interactions ε (such as the amplitude of surface roughness). If these particles are made to move past the obstacle with
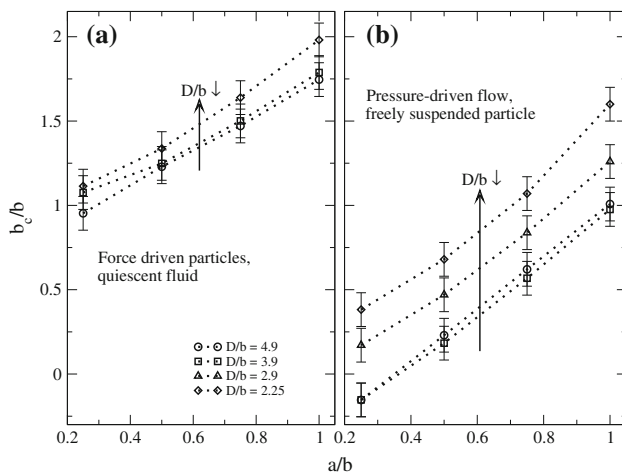
Fig. 5 The critical offset b_c as a function of the particle radius. The critical offset is evaluated at $\varepsilon = 0.05$ by linear interpolation between two simulated trajectories for each particle size, leading to the *error bars* in the plots. **a** A constant force drives the particles past the obstacle in a quiescent fluid, **b** a constant pressure drop drives the fluid carrying the particle past the obstacle

the same initial offset satisfying $b_{c1} < b_{in} < b_{c2}$, the larger particle would get displaced onto the critical trajectory and would travel with a final offset b_{c2}, while the smaller particle would not get affected by the non-hydrodynamic interactions and continue to a final offset b_{in}, thus separating the two particles spatially, along the z-direction. Another possibility would be an initial offset satisfying $b_{in} < b_{c1} < b_{c2}$, which leads to separation since both particles would move along the corresponding critical trajectories downstream to the obstacle. The lateral displacement between the two particles in this case is $(b_{c2} - b_{c1})$ and is larger than that in the previous case (i.e., $b_{c2} - b_{in}$). Therefore, the spatial resolution of separation in this latter case is maximum. As shown in Fig. 5, the critical offset is more sensitive to changes in particle radii in the pressure-driven case than in the case of a constant force. Therefore, the spatial resolution would be higher between the two particles in the pressure-driven case.

5 Summary

In summary, we have studied the behavior of spherical particles of different sizes moving in a channel through a constriction between a fixed spherical obstacle and a plane wall. We have investigated cases pertaining to different particle-to-obstacle aspect ratios and constriction apertures. We observe that the particles reach closer to the obstacle as the particle size increases or the constriction aperture reduces in size. Our simulations also show that a particle driven by a constant force in a quiescent fluid reaches

closer to the obstacle than one freely suspended in a pressure-driven flow. However, in the case of a pressure-driven flow, we observe a larger range of change in b_c. We have discussed the implications of these observations assuming that a hard-wall potential model fairly represents the repulsive non-hydrodynamic interactions. We have inferred that a particle reaching closer to the obstacle is equivalent to increasing the critical offset associated with the particle. Therefore, the observed dependence of the critical offset on the particle size serves as the basis for size-based separation. Finally, the separation resolution is higher in the case of a fluid flow driving the particles, compared to a constant driving force in a quiescent fluid.

References

Ashley JF, Bowman CN, Davis RH (2013) Hydrodynamic separation of particles using pinched-flow fractionation. AIChE J 59(9):3444–3457

Balvin M, Sohn E, Iracki T, Drazer G, Frechette J (2009) Directional locking and the role of irreversible interactions in deterministic hydrodynamics separations in microfluidic devices. Phys Rev Lett 103:078301

Bowman T, Frechette J, Drazer G (2012) Force driven separation of drops by deterministic lateral displacement. Lab Chip 12:2903–2908

Devendra R, Drazer G (2012) Force driven deterministic lateral displacement for particle separation in microfluidic devices. Anal Chem 84:10621–10627

Faivre M, Abkarian M, Bickraj K, Stone HA (2006) Geometrical focusing of cells in a microfluidic device: an approach to separate blood plasma. Biorheology 43:147–159

Frechette J, Drazer G (2009) Directional locking and deterministic separation in periodic arrays. J Fluid Mech 627:379–401

Han J, Craighead HG (2000) Separation of long DNA molecules in a microfabricated entropic trap array. Science 288(5468):1026–1029

Huang LR, Cox EC, Austin RH, Sturm JC (2004) Continuous particle separation through deterministic lateral displacement. Science 304(5673):987–990

Ladd AJC (1994a) Numerical simulations of particulate suspensions via a discretized boltzmann equation. Part 1. Theoretical foundation. J Fluid Mech 271:285–309

Ladd AJC (1994b) Numerical simulations of particulate suspensions via a discretized boltzmann equation. Part 2. Numerical results. J Fluid Mech 271:311–339

Larsen AV, Poulsen L, Birgens H, Dufva M, Kristensen A (2008) Pinched flow fractionation devices for detection of single nucleotide polymorphisms. Lab Chip 8(5):818–821

Lee KH, Kim SB, Lee KS, Sung HJ (2011) Enhancement by optical force of separation in pinched flow fractionation. Lab Chip 11(2):354–357

Luo M, Sweeney F, Risbud SR, Drazer G, Frechette J (2011) Irreversibility and pinching in deterministic particle separation. Appl Phys Lett 99(6):064102

Maenaka H, Yamada M, Yasuda M, Seki M (2008) Continuous and size-dependent sorting of emulsion droplets using hydrodynamics in pinched microchannels. Langmuir 24:4405–4410

Morijiri T, Sunahiro S, Senaha M, Yamada M, Seki M (2011) Sedimentation pinched-flow fractionation for size-and density-based particle sorting in microchannels. Microfluid Nanofluid 11(1):105–110

Mortensen NA (2007) Comment on pinched flow fractionation: continuous size separation of particles utilizing a laminar flow profile in a pinched microchannel. Anal Chem 79:9240–9241

Mustin B, Stoeber B (2010) Deposition of particles from polydisperse suspensions in microfluidic systems. Microfluid Nanofluid 9:905–913

Nguyen NQ, Ladd AJC (2002) Lubrication corrections for lattice-Boltzmann simulations of particle suspensions. Phys Rev E 66:046708

Risbud SR, Drazer G (2013) Trajectory and distribution of non-Brownian suspended particles moving past a fixed spherical or cylindrical obstacle. J Fluid Mech 714:213–237

Risbud SR, Luo M, Frechette J, Drazer G (2013) Analysis of the trajectory of a sphere moving through a geometric constriction. Phys Fluids 25:062001

Shardt O, Mitra SK, Derksen JJ (2012) Lattice boltzmann simulations of pinched flow fractionation. Chem Eng Sci 75:106–119

Vig AL, Kristensen A (2008) Separation enhancement in pinched flow fractionation. Appl Phys Lett 93:203507

Wyss HM, Blair DL, Morris JF, Stone HA, Weitz DA (2006) Mechanism for clogging of microchannels. Phys Rev E 74:061402

Xuan X, Zhu J, Church C (2010) Particle focusing in microfluidic devices. Microfluid Nanofluid 9(1):1–16

Yamada M, Nakashima M, Seki M (2004) Pinched flow fractionation: continuous size separation of particles utilizing a laminar flow profile in a pinched microchannel. Anal Chem 76(18):5465–5471